The Canadian Mineralogist
Vol. 36, pp. 415-431 (1998)

COMPOSITIONAL VARIATION OF TOURMALINE IN THE GRANITIC PEGMATITE DYKES OF THE CRUZEIRO MINE, MINAS GERAIS, BRAZIL

MARCELLA FEDERICO, GIOVANNI B. ANDREOZZI, SERGIO LUCCHESI[1] AND GIORGIO GRAZIANI

Dipartimento di Scienze della Terra, Università di Roma "La Sapienza", P.le A. Moro, 5, I-00185 Roma, Italia

JÚLIO CÉSAR-MENDES[2]

DEGEO, Escola de Minas, UFOP, Campus do Morro do Cruzeiro, 35400-000, Ouro Preto, Minas Gerais, Brasil

ABSTRACT

Schorl – dravite and schorl – elbaite from different zones of the rare-element-enriched complex granitic pegmatite dykes of the Cruzeiro mine, in Minas Gerais, Brazil, were analyzed by electron and ion (H, Li, B) microprobes. *General* mechanisms of substitution (common to schorl and to elbaite independently of their position in the pegmatites) drive compositions to "proton-deficient schorl", "alkali-free schorl", and "alkali-free elbaite" end-members, each involving Al enrichment. Among the *specific* mechanisms (*i.e.*, those characterizing tourmaline within each separate zone), "octahedral-defect" and "alkali-free proton-rich" types are particularly important in OH-rich, pocket elbaite. The substitution $^{X}\square + OH^{-} \leftrightarrow {}^{X}Na^{+} + O^{2-}$, driving compositions to an "alkali-free proton-rich elbaite", is proposed to explain both the lack of Na and the excess of (OH + F). Bond-valence calculations based on results of unpublished structure-refinement data allow the OH excess to be assigned to the O(2) site. The composition of the tourmaline in the Cruzeiro suite (high Al content; Mg, Fe, Zn, Mn, and Li covariation; antithetic behavior of OH and F) records the evolution of the pegmatite-forming melt.

Keywords: tourmaline, crystal chemistry, mechanisms of substitution, hydroxyl excess, alkali-free proton-rich elbaite, granitic pegmatites, Cruzeiro mine, Minas Gerais, Brazil.

SOMMAIRE

Nous avons analysé, au moyen de microsondes électronique et ionique (H, Li, B), la tourmaline des séries schorl – dravite et schorl – elbaïte provenant des diverses zones des pegmatites granitiques à éléments rares exploitées pour la tourmaline à la mine Cruzeiro, au Minas Gerais, Brésil. Les mécanismes de substitution *généraux* (ceux qui sont communs au schorl et à l'elbaïte indépendamment de leur position dans les pegmatites) conduisent aux pôles "schorl déficitaire en protons", "schorl dépourvu d'alcalins", et "elbaïte dépourvue d'alcalins", chacun de ceux-ci contribuant à un enrichissement en Al. Parmi les mécanismes *spécifiques*, ceux qui caractérisent la variation de la tourmaline au sein d'une seule zone, les schémas impliquant les lacunes dans les sites octaédriques et les déficits en alcalins à la faveur d'un enrichissement en protons sont particulièment importants dans l'elbaïte provenant des cavités miarolitiques, milieux riches en OH. La substitution $^{X}\square + OH^{-} \leftrightarrow {}^{X}Na^{+} + O^{2-}$, qui mène à l'elbaïte sans alcalins et riche en protons, serait à l'origine à la fois du manque en Na et de l'excès en (OH + F). Les valeurs des valences de liaison, calculées à partir des résultats non publiés d'analyses de la structure cristalline de ces échantillons, nous permettent d'attribuer l'excédent en OH au site O(2). La composition de la tourmaline dans la suite de Cruzeiro (teneur élevée en Al; covariation en Mg, Fe, Zn, Mn, et Li, variation antithétique des proportions de OH et de F) témoignent de l'évolution du magma qui a cristallisé sous forme de pegmatites granitiques.

(Traduit par la Rédaction)

Mots-clés: tourmaline, chimie cristalline, mécanismes de substitution, excédent en hydroxyle, elbaïte riche en protons et sans alcalins, pegmatites granitiques, mine de Cruzeiro, Minas Gerais, Brésil.

INTRODUCTION

Minerals of the tourmaline group have been studied extensively because of their complex composition, structure and importance as petrological indicators. Their systematic compositional variations are related to the P–T–*X*–$f(O_2)$ conditions of the environment of crystallization and to interactions with the host rocks (Henry & Guidotti 1985, Shearer *et al.* 1986). This is especially the case for granitic pegmatites in which the sensitivity of tourmaline to the activity of Fe, Mg, Al, and Mn makes them recorders of internal evolution

[1] *E-mail address*: graziani@axrma.uniroma1.it
[2] *E-mail address*: julio@degeo.ufop.br

(Staaz *et al.* 1955, Foord 1977, Walker *et al.* 1986, Jolliff *et al.* 1986, Foord *et al.* 1989).

In this paper, the first part of a general study of tourmaline from deposits in the Cruzeiro granitic pegmatites, our objective is to clarify some aspects of the mechanisms of chemical variation in tourmaline during crystallization of the pegmatite. The second part will focus on the crystal chemistry of the tourmaline group.

The Cruzeiro dykes are rare-element-enriched complex pegmatites with distinct horizontal and vertical zoning, and strong enrichment in Li, F and Rb in the upper parts (César-Mendes 1995, César-Mendes & Svisero 1992, 1994, César-Mendes *et al.* 1993a, b). The characteristics that led to the choice of the Cruzeiro pegmatites as the source of tourmaline for this study are: (1) their well-defined zoning, (2) the abundance of tourmaline, and (3) the presence of quartzite as the host rock. The latter suggests limited interaction with the pegmatite-forming melt. Thus the chemical composition and mechanisms of substitution in these samples of tourmaline can be expected to be exclusively dependent on the composition of the melt and the local conditions of its crystallization.

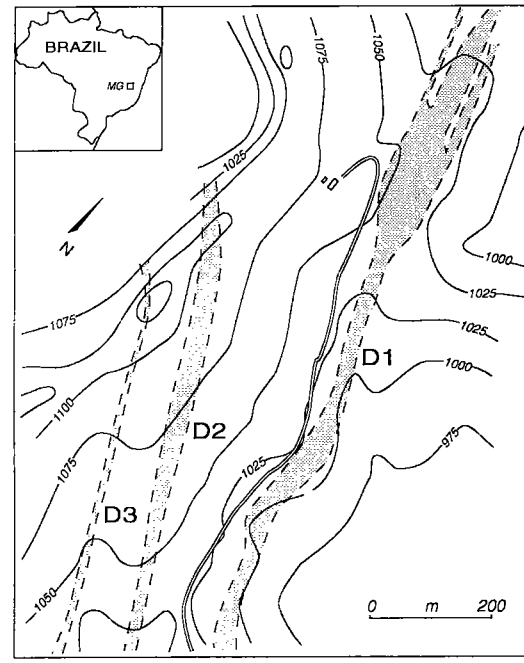

FIG. 1. Sketch of the Cruzeiro area. D1: Dyke 1, D2: Dyke 2, D3: Dyke 3 (from Cassedanne *et al.* 1980).

GEOLOGICAL SETTING AND REGIONAL PETROGRAPHY

The Cruzeiro mine is located 13.5 km northwest of the small village of São José da Safira, near Governador Valadares, in the eastern center of the Brazilian state of Minas Gerais (César-Mendes 1995). The pegmatite dykes (Fig. 1) are emplaced in a quartzite of the Serra da Safira sequence. This sequence may be described, from base to top, as gently west-dipping layers of meta-ultramafic schists, of metapelitic schists, and of a coarse-grained quartzite several hundred meters thick (Cassedanne *et al.* 1980). This sequence overlies a regional lithostructural unit, the Gneiss Piedade, composed of gneiss, quartzite and schist (Silva *et al.* 1987). The mineral assemblages in the rocks of the São José da Safira region are indicative of the middle amphibolite facies. Although granite was not found in the surrounding area, the pegmatite bodies of the region may be derived from a granitic pluton. The emplacement of the pegmatites seems to have been controlled by regional structure, as indicated by the concentration of many bodies along lineaments oriented N10–20°W (César-Mendes & Jordt-Evangelista 1994).

INTERNAL STRUCTURE OF THE PEGMATITE DYKES

The three subvertical, parallel dykes (Fig. 1), running N20°W and intruding 80–86°SW, have sharply defined contacts with the host quartzite. The first (dyke 1) is 1300 m long and up to 60 m wide, the second, now inaccessible, is 900 m long and about 20 m wide, and the third (dyke 3) is 700 m long with a maximum width of 8 m in outcrop. Their internal characteristics are essentially similar: according to the different assemblages of minerals (Table 1), the dykes show symmetrical development around a quartz core and a horizontal zoning. This zoning consists of a border zone, a wall zone, an intermediate zone and a core (César-Mendes 1995).

The *border zone* (hereafter referred to as *Bz*) is normally of very limited thickness, ranging from 3 to 5 cm and rarely exceeding 10 cm. The *wall zone* (*Wz*) gradually evolves from the *Bz*, and its thickness varies in direct proportion to the thickness of the pegmatite body. In dyke 1, it reaches about 1 m, whereas in dyke 3 it is thinner. The *intermediate zone* is economically the most important, as it produces colored tourmaline. In dyke 1, this zone can be further subdivided into *external*, *medium* and *internal*; in the smaller dyke 3, the zone can be divided into only two parts, external and internal. In dyke 1, the *external intermediate zone* (*EIz*) is characterized by an increase in grain size. The *medium intermediate zone* (*MIz*) is a transitional layer that was locally subject to late metasomatic processes. The *internal intermediate zone* (*IIz*) grades into the core. Pockets (*P*), or miarolitic cavities, are found in the *IIz* of all dykes near their cores. The *core* (*C*) is discontinuous and is composed mainly of milky quartz; no tourmaline was found.

TABLE 1. SAMPLE DISTRIBUTION OF THE TOURMALINES FROM THE CRUZEIRO PEGMATITE DYKES

Zones	No. of crystals and grains analyzed	No. of EMP analyses performed	Paragenesis	Tourmaline abundance, textural characteristics and bulk color
Border (*Bz*)	14	50	Fine-grained mixture of feldspar, quartz and muscovite; minor alkali-poor beryl, almandine-rich garnet and niobiotantalates	Minor; subhedral crystals intensely fractured; black
Wall (*Wz*)	75	353	Medium-grained mixture of feldspar, large muscovite sheets and interstitial quartz	Subordinate; subhedral crystals intensely fractured; black
External intermediate (*Elz*)	17	199	Coarse-grained mixture of quartz, feldspar and minor muscovite	Sporadic; medium-grained subhedral crystals; black, black-green zoned
Medium intermediate (*Mlz*)	16	68	Muscovite books, quartz and feldspar	Medium-grained; subhedral crystals; black, green
Internal intermediate (*Ilz*)	37	372	Feldspar, "cleavelandite", large tabular pink muscovite, quartz and spodumene; subordinate manganotantalite and sporadic light pink muscovite	Abundant; subhedral crystals of big to enormous size; black with green-blue rim, green, pink
Pockets (*P*)	10	682	Quartz, "cleavelandite", pink muscovite, lepidolite, spodumene; subordinate spessartine-rich garnet and pink beryl	Euhedral crystals; transparent, green, pink and color zoned
Core (*C*)	-	-	Quartz, feldspar and mica	-

EXPERIMENTAL

A large number of small black grains of fractured tourmaline from the outer zones of the pegmatites and several prismatic, colored crystals from their inner zones were hand-picked, representative of the core–rim zoning, where present.

X-ray diffraction

Unit-cell parameters were determined with a Siemens *P*4 single-crystal diffractometer, with Mo$K\alpha_1$ radiation, using 26 independent reflections and their Friedel pairs, from 85 to 95°2θ, after a preliminary orientation, matrix calculation and indexing.

Analytical procedures

Electron-microprobe analysis (EMPA): Tourmaline compositions were determined with a Cameca SX–50 operated with five wavelength-dispersion (WDS) spectrometers and a Link eXL energy-dispersion system (EDS), both controlled by Specta software, at the "Centro di Studio per il Quaternario e l'Evoluzione Ambientale", C.N.R., Roma, Italy. Data were reduced with the ZAF–4/FLS software. Operating conditions were as follows: accelerating voltage 15 kV, sample current 15 nA, 100 and 20 s counting time for EDS and WDS determinations, respectively. The natural and synthetic standards were: wollastonite (Si, Ca), corundum (Al), jadeite (Na), periclase (Mg), fluorphlogopite (F), magnetite (Fe), orthoclase (K), rutile (Ti), metallic Mn and Zn. Average experimental errors (wt.%) were: SiO_2 0.18; TiO_2 0.03; Al_2O_3 0.18; FeO 0.20 (schorl), 0.10 (elbaite), MnO 0.09, MgO 0.10, ZnO 0.09, CaO 0.05, Na_2O 0.05, K_2O 0.02, F 0.04 (schorl), 0.10 (elbaite).

Ion-microprobe analysis (SIMS): The SIMS (Secondary-Ion Mass Spectrometry) analysis was done with a Cameca IMS–3f instrument, for measurement of H, Li, B, Be, C and N contents, at the "Centre de Recherches Pétrographiques et Géochimiques", C.N.R.S., Nancy, France. Experimental conditions were: primary current of oxygen negative, with an intensity of 5 nA, focused on 10 μm; secondary current of positive ions; voltage offset of –60 V, energy window of 10 V. Measurements were carried out with an electron multiplier in counting mode and with automatic centering of the magnetic field (Deloule *et al.* 1992). Average experimental errors (wt.%) were: B_2O_3 0.56, Li_2O 0.10 (elbaite), H_2O 0.16.

The H and Li values, obtained using the calibration curves with some glasses and one schorl–dravite tourmaline as standards, did not match the data previously obtained through replicate analysis using TG (H) and AAS (Li) techniques. The latter determinations were done on unzoned crystals of the suite for which sufficient material was available. Checks subsequently made on the above mentioned standards provided evidence that the SIMS data were

affected by matrix effects, caused by the difference in silica content between glass and tourmaline, as reported for Li by Wilson & Long (1983). This finding suggested that the compositional difference between the schorl–dravite standard and the elbaitic samples could cause systematic errors, and implied that it would be necessary to use an external procedure of standardization. For this reason, the SIMS measurements were calibrated with the TG and AAS data.

For B measurement, no matrix effect due to silica was observed using a calibration curve with glasses and tourmaline standards. However, two clusters were shown by measurements of Fe-rich and Fe-free tourmalines, respectively. This suggested a matrix effect due to iron content (L. Ottolini, pers. commun.). For this reason, two calibration curves were used, based on glasses for Fe-free samples and on the schorl–dravite standard for Fe-rich samples.

The presence of Be, C and N was tested to establish whether they are significant for possible substitution at the boron site. However, the results obtained did not support this conjecture, as Be content reached only a maximum of 15 ppm, and C and N were practically absent.

Atomic absorption spectroscopy (AAS): Analysis for Li was done also by AAS. Samples were dissolved using a solution of HF and H_2SO_4 in an autoclave operating at 150°C for 4 h. One reference sample of homogeneous elbaite from Espiritu Santo, Brazil, was analyzed several times to quantify the experimental reproducibility: its mean Li_2O content was found to be 2.08(12) wt.%.

Thermal analysis: Thermal analysis (TG and DTA) was done to measure H_2O contents using a Setaram TAG 24 instrument operating at the following conditions: heating rate 10°C/mn, nitrogen atmosphere, sample weight about 10 mg, alumina crucible, calcined alumina as inert material.

Ferrous iron determination: The determination was done by titration method using $KMnO_4$. Samples were dissolved with a solution of HF and H_2SO_4 in a Milestone MLS 1200 Mega microwave-digestion system, operating for 1 h; a nitrogen atmosphere was used to minimize oxidation.

Distribution, Occurrence, Texture of Tourmaline

The Cruzeiro pegmatites contain euhedral prisms of schorl to variously colored elbaite (Table 1), a sequence that is not frequently found in the pegmatites of Brazil. Crystal dimensions range from some centimeters to one meter in length, but unfortunately the large prismatic crystals observed *in situ* could not be sampled because of their intense fracturing, particularly the schorl, so that only small fragments or occasional small euhedral crystals could be extracted.

Samples from dyke 1 were collected from the João de Matos and the Descarga adits; the former completely crosses the dyke and allows examination of the almost perfect symmetry of the zones in the western and eastern sides. Samples from dyke 3 were collected from the Ladim adit that ends at the pegmatite core. Tourmaline crystals are ubiquitous, and are particularly abundant in the *IIz* and the pockets. Tourmaline composition varies from outer to inner zones, in accord with the change in color from black to green and, locally, to pink. On the other hand, there is no tourmaline in the quartz core.

The *Bz* and *Wz* contain centimetric black tourmaline crystals. The prisms commonly appear with the **c** axis orthogonal to the contact with the country rock. They are intensely fractured, with the fracture plane subnormal to the **c** axis.

The *EIz* and *MIz* contain black tourmaline crystals that vary considerably in size, mostly subnormal to the contact between the zones. In dyke 1, color-zoned crystals, such as sample 84 with a black core and green rim, are occasionally found in areas subject to late fluid–rock interaction.

Tourmaline crystals from the *IIz* of dyke 1 are centimetric to decimetric, transparent, and deep pink and green, whereas those from pockets are smaller, euhedral, transparent, homogeneous in color, green, light green and deep pink (samples 65, 60, 61 R, respectively), or core–mantle–rim zoned, characterized by different hues of green (samples 62 and 64).

Tourmaline crystals from the intermediate zone of dyke 3 generally occur as enormous, black prisms up to one meter long and 30 centimeters wide, locally with a narrow blue-green rim, and attain up to 30 vol.% toward the core. Moreover, some small color-zoned prisms also were found, such as sample 93 with a black core and a deep-blue rim. Prisms from the pockets are green and blue, euhedral and inclusion-free, such as sample 95 (whose core is labeled 95V).

Unit-Cell Dimensions

Unit-cell dimensions of samples from dyke 1 (Fig. 2) plot close to the elbaite–schorl join (Deer *et al.* 1986). Tourmaline from *Bz* and *MIz* plots close to the schorl end-member, whereas *IIz* and pocket tourmaline is close to, or exactly at, the elbaite end of the join. In particular, tourmaline from the *Wz* and the *EIz* shows evidence of a dravitic trend.

Compositional Relations

The chemical composition of the Cruzeiro tourmaline was investigated in detail on more than 150 samples with over 1500 electron-microprobe analyses (Fig. 3, Table 1). These samples consist of crystalline fragments (from 1 to 3 mm) and {0001} sections; they were analyzed at random spots and along traverses (no less than 100 μm steps), respectively. The data provide

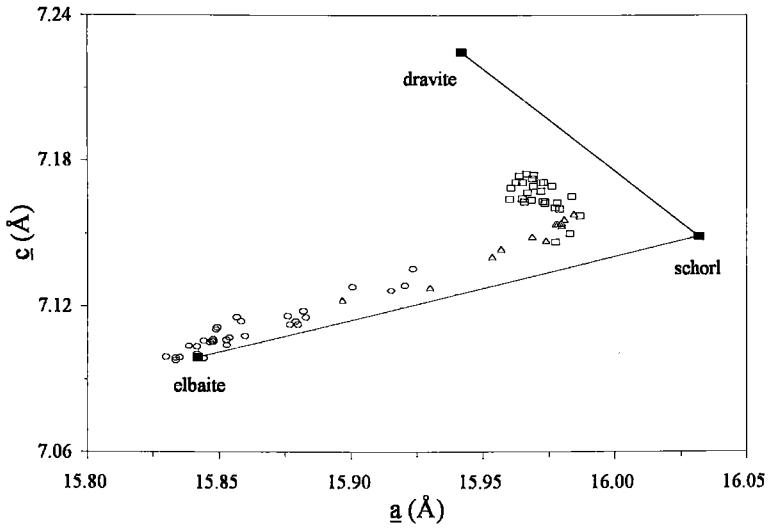

FIG. 2. Unit-cell dimensions of tourmaline crystals from the Cruzeiro granitic pegmatite suite. Reference lines according to Deer *et al.* (1986). Open triangles: tourmalines from *Bz* and *Mlz*. Open squares: tourmalines from *Wz* and *Elz*. Open circles: tourmalines from *Ilz* and pockets. The dimensions of the symbols used correspond to about four times the average experimental error.

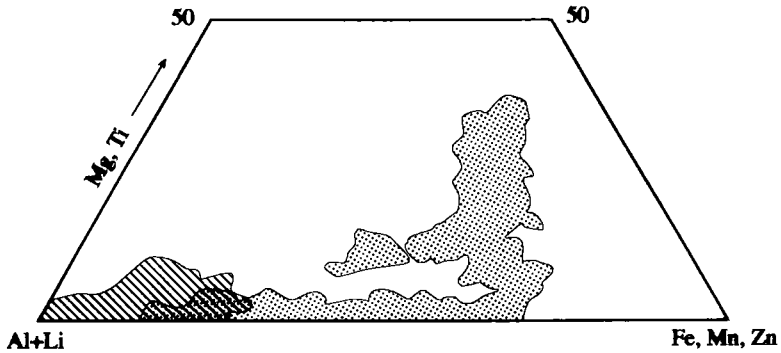

FIG. 3. Compositions of tourmaline from the Cruzeiro granitic pegmatite suite, in terms of (Al + Li) – (Fe, Mn, Zn) – (Mg, Ti), *i.e.*, atomic proportions of the *Y*-site cations (Jolliff *et al.* 1986). Dotted area: tourmalines from *Bz* to *Mlz*. Striped area: tourmalines from *Ilz* and pockets.

TABLE 2. REPRESENTATIVE ELECTRON AND ION MICROPROBE DATA OF TOURMALINES FROM THE ZONES OF THE CRUZEIRO PEGMATITE DYKE 1

Zones	*West Bz*	*Wz*			*Elz*	*Mlz*		*Ilz*			*P*			*Ilz*			*Mlz*	*Elz*	*Wz*			*East Bz*
Samples	68 A	68 B	70	71 E	71 B	72 D	72	80 A	80 B	80 C	65	61 R	60	75	75 A	75B	76	77 C	77	77 L	79 A	79
SiO_2	34.31	34.52	34.57	35.94	35.18	35.39	34.42	36.83	35.58	37.78	36.63	38.82	38.01	38.21	37.98	37.66	34.56	35.16	35.38	35.60	35.52	34.66
TiO_2	0.19	0.39	0.31	0.48	0.18	0.29	0.16	0.12	-	-	-	-	-	0.13	0.16	0.34	0.22	0.24	0.36	0.47	0.44	0.22
B_2O_3	10.14	10.18	10.19	10.50	10.33	10.38	10.13	10.68	10.36	10.91	10.59	11.14	10.96	11.01	10.95	10.88	10.19	10.33	10.38	10.42	10.41	10.21
Al_2O_3	33.82	34.70	33.60	33.08	33.22	32.95	34.27	36.89	37.31	40.19	38.52	41.64	40.53	39.66	38.14	37.63	33.48	33.93	33.67	33.21	33.45	34.19
FeO	14.34	12.10	12.62	11.00	12.72	13.68	14.60	6.20	3.90	1.51	2.61	-	1.27	2.28	3.65	5.26	14.76	13.58	10.94	10.61	10.44	13.53
MnO	0.31	0.64	0.15	0.19	0.22	0.33	0.48	1.24	1.98	0.47	2.76	0.82	0.23	0.41	0.30	0.42	0.47	0.57	0.12	0.17	-	0.39
MgO	1.10	1.62	2.61	3.49	2.51	1.91	0.28	-	-	0.14	0.20	-	-	0.64	0.89	0.74	0.43	0.93	3.77	3.99	3.73	1.24
ZnO	0.20	0.15	0.37	0.24	0.22	0.33	0.41	0.86	1.72	-	1.70	-	0.17	-	0.09	-	0.55	0.24	0.16	0.17	0.20	0.25
CaO	0.33	0.40	0.19	0.20	0.18	0.07	-	0.04	0.19	0.45	0.12	0.15	0.18	0.14	0.17	0.12	0.03	0.07	0.15	0.13	0.17	0.03
Na_2O	1.96	1.90	1.97	2.11	1.99	2.00	1.64	2.49	2.74	1.99	2.27	1.86	2.03	2.24	2.49	2.54	1.83	1.78	2.21	2.13	2.09	1.75
K_2O	0.08	0.03	0.04	0.04	0.04	0.05	0.07	0.02	0.02	0.01	0.02	-	0.02	0.02	0.02	0.03	0.05	0.04	0.05	0.05	0.07	0.03
Li_2O	0.06	0.26	0.03	0.09	0.08	0.04	0.13	1.23	1.45	1.83	1.21	2.08	1.96	1.66	1.64	1.27	0.21	0.10	0.05	0.10	0.23	0.07
F	0.55	0.41	0.27	0.34	0.38	0.32	0.44	1.36	1.56	1.13	0.92	0.93	1.06	1.18	1.27	1.19	0.39	0.44	0.42	0.43	0.43	0.32
H_2O	3.01	3.02	3.01	3.02	3.01	3.02	2.98	3.03	3.03	3.17	3.23	3.60	3.40	3.27	3.26	3.15	2.96	2.99	3.01	3.07	3.02	3.02
Sum	100.39	100.32	99.92	100.71	100.26	100.75	100.01	100.98	99.84	99.57	100.77	101.04	99.82	100.85	101.01	101.24	100.14	100.40	100.67	100.53	100.19	99.90
O≡F	-0.23	-0.17	-0.11	-0.14	-0.16	-0.14	-0.19	-0.57	-0.66	-0.47	-0.39	-0.39	-0.45	-0.50	-0.53	-0.50	-0.17	-0.18	-0.18	-0.18	-0.18	-0.13
Total	100.16	100.15	99.81	100.57	100.10	100.61	99.82	100.41	99.18	99.09	100.38	100.65	99.37	100.35	100.47	100.74	99.98	100.22	100.49	100.35	100.01	99.77
											Number of ions on the basis of 31 (O,OH,F)											
Si	5.830	5.785	5.859	5.974	5.925	5.957	5.870	5.985	5.850	5.977	5.919	6.007	5.994	6.016	6.023	6.019	5.901	5.940	5.902	5.932	5.929	5.881
Al(*T*)	0.170	0.215	0.141	0.026	0.075	0.043	0.130	0.015	0.150	0.023	0.081	0.000	0.006	0.000	0.000	0.000	0.099	0.060	0.098	0.068	0.071	0.119
B	2.985	3.047	2.981	3.058	3.032	3.049	2.982	2.995	2.940	3.058	2.953	2.964	2.983	2.992	2.997	3.001	3.002	3.011	2.988	2.997	2.999	2.990
Al(*Z*)	6.000	6.000	6.000	6.000	6.000	6.000	6.000	6.000	6.000	6.000	6.000	6.000	6.000	6.000	6.000	6.000	6.000	6.000	6.000	6.000	6.000	6.000
Al(*Y*)	0.605	0.641	0.571	0.456	0.520	0.496	0.760	1.052	1.083	1.474	1.257	1.597	1.530	1.362	1.131	1.091	0.639	0.697	0.524	0.456	0.512	0.722
Fe	2.037	1.696	1.789	1.530	1.791	1.926	2.083	0.843	0.536	0.200	0.353	0.000	0.167	0.301	0.484	0.703	2.107	1.918	1.527	1.479	1.458	1.921
Ti	0.024	0.049	0.039	0.060	0.023	0.037	0.021	0.014	0.000	0.000	0.000	0.000	0.000	0.015	0.020	0.041	0.028	0.031	0.045	0.059	0.055	0.028
Mn	0.045	0.091	0.021	0.027	0.032	0.047	0.069	0.170	0.276	0.064	0.378	0.107	0.031	0.055	0.040	0.057	0.068	0.082	0.017	0.024	0.000	0.056
Mg	0.280	0.405	0.660	0.865	0.629	0.480	0.071	0.000	0.000	0.032	0.047	0.000	0.000	0.150	0.211	0.176	0.110	0.235	0.937	0.990	0.929	0.313
Zn	0.025	0.019	0.046	0.029	0.027	0.041	0.052	0.103	0.208	0.000	0.202	0.000	0.019	0.000	0.010	0.000	0.070	0.030	0.019	0.021	0.025	0.031
Li	0.043	0.175	0.020	0.060	0.054	0.027	0.088	0.806	0.958	1.165	0.786	1.295	1.243	1.051	1.047	0.817	0.143	0.067	0.034	0.066	0.154	0.047
Y tot.	3.058	3.075	3.146	3.027	3.075	3.054	3.143	2.988	3.061	2.934	3.024	2.999	2.991	2.935	2.943	2.884	3.165	3.059	3.102	3.095	3.133	3.117
Ca	0.061	0.072	0.035	0.035	0.032	0.013	0.000	0.007	0.033	0.075	0.020	0.025	0.030	0.023	0.029	0.021	0.005	0.013	0.028	0.022	0.031	0.005
Na	0.647	0.617	0.648	0.680	0.651	0.653	0.543	0.785	0.874	0.609	0.712	0.558	0.620	0.682	0.766	0.788	0.607	0.583	0.715	0.689	0.674	0.577
K	0.017	0.006	0.010	0.008	0.009	0.010	0.015	0.003	0.005	0.002	0.004	0.000	0.003	0.004	0.005	0.006	0.011	0.010	0.010	0.010	0.014	0.006
X tot.	0.724	0.696	0.692	0.723	0.693	0.675	0.559	0.796	0.912	0.687	0.736	0.583	0.654	0.710	0.799	0.815	0.624	0.606	0.753	0.722	0.719	0.588
OH	3.410	3.376	3.403	3.347	3.386	3.386	3.385	3.281	3.324	3.346	3.481	3.716	3.576	3.431	3.449	3.358	3.372	3.365	3.349	3.412	3.363	3.419
F	0.293	0.217	0.144	0.179	0.204	0.171	0.239	0.696	0.812	0.563	0.469	0.455	0.529	0.588	0.635	0.604	0.212	0.233	0.221	0.225	0.225	0.170
OH+F	3.703	3.593	3.547	3.527	3.590	3.557	3.624	3.977	4.136	3.909	3.950	4.171	4.106	4.019	4.084	3.962	3.583	3.598	3.570	3.636	3.589	3.589

B_2O_3, Li_2O and H_2O from ion microprobe. Total iron as FeO. - : Below detection limit. See text for average experimental errors.

TABLE 3. REPRESENTATIVE ELECTRON AND ION MICROPROBE DATA OF TOURMALINES FROM THE ZONES OF THE CRUZEIRO PEGMATITE DYKE 3

Zones	*Bz*	*Wz*			*Elz*	*Ilz*			*P*
Samples	88 A	88	90 A	90	91	92 F	92 D	92 E	95 V
SiO_2	35.40	34.71	34.97	34.48	34.25	36.16	36.50	37.55	37.48
TiO_2	0.27	0.32	0.20	0.11	0.25	0.11	-	-	-
B_2O_3	10.38	10.23	10.28	10.18	10.12	10.55	10.63	10.86	10.84
Al_2O_3	33.50	33.46	33.89	35.28	34.99	35.89	37.63	40.15	37.81
FeO	13.40	11.70	14.21	12.21	11.52	8.45	5.23	1.16	3.39
MnO	0.30	0.12	0.46	0.97	0.32	1.31	1.41	1.98	2.09
MgO	1.04	3.14	0.43	0.08	1.48	0.25	0.14	-	-
ZnO	0.27	0.30	0.34	0.67	0.23	0.33	0.25	0.10	0.27
CaO	0.19	0.13	0.07	0.12	0.53	0.09	0.15	0.28	0.34
Na_2O	1.91	2.16	1.76	1.99	1.95	2.38	2.61	2.16	2.51
K_2O	0.04	0.04	0.02	0.05	0.04	0.02	0.04	0.03	0.06
Li_2O	0.15	0.02	0.13	0.45	0.41	0.88	1.31	1.86	1.58
F	0.43	0.40	0.45	0.49	0.62	0.99	1.26	1.33	1.49
H_2O	2.96	3.11	3.08	3.03	2.88	2.94	2.99	3.07	3.34
Sum	100.23	99.85	100.28	100.10	99.59	100.35	100.17	100.53	101.20
O≡F	-0.18	-0.17	-0.19	-0.20	-0.26	-0.42	-0.53	-0.56	-0.63
Total	100.05	99.68	100.09	99.90	99.33	99.93	99.63	99.97	100.57
Number of ions on the basis of 31 (O,OH,F)									
Si	5.982	5.859	5.924	5.829	5.798	5.975	5.945	5.956	5.984
Al(*T*)	0.018	0.141	0.076	0.171	0.202	0.025	0.055	0.044	0.016
B	3.027	2.980	3.006	2.970	2.956	3.008	2.987	2.973	2.986
Al(*Z*)	6.000	6.000	6.000	6.000	6.000	6.000	6.000	6.000	6.000
Al(*Y*)	0.656	0.517	0.693	0.861	0.781	0.966	1.169	1.464	1.099
Fe	1.894	1.651	2.013	1.726	1.631	1.168	0.712	0.154	0.452
Ti	0.034	0.041	0.025	0.014	0.031	0.013	0.000	0.000	0.000
Mn	0.043	0.017	0.066	0.139	0.046	0.183	0.194	0.266	0.283
Mg	0.262	0.791	0.108	0.020	0.373	0.060	0.035	0.000	0.000
Zn	0.033	0.038	0.043	0.084	0.029	0.040	0.031	0.012	0.032
Li	0.100	0.014	0.087	0.303	0.288	0.586	0.860	1.188	1.014
Y tot.	3.023	3.069	3.035	3.146	3.178	3.018	3.000	3.083	2.879
Ca	0.035	0.023	0.014	0.022	0.095	0.015	0.026	0.048	0.058
Na	0.626	0.708	0.579	0.652	0.640	0.764	0.824	0.664	0.777
K	0.008	0.009	0.005	0.011	0.009	0.005	0.009	0.005	0.011
X tot.	0.669	0.740	0.598	0.684	0.745	0.784	0.859	0.718	0.847
OH	3.336	3.502	3.478	3.417	3.252	3.241	3.247	3.252	3.557
F	0.227	0.215	0.241	0.259	0.332	0.518	0.651	0.666	0.751
OH+F	3.563	3.717	3.719	3.676	3.584	3.758	3.898	3.917	4.308

B_2O_3, Li_2O and H_2O from ion microprobe. Total iron as FeO. - : Below detection limit. See text for average experimental errors.

evidence of almost homogeneous compositions within each single fragment of tourmaline. Locally, however, chemical variations were found among samples belonging to the same pegmatite zone owing to the presence of large zoned crystals, which subsequently fractured. This is indirectly confirmed by a clearly visible color zoning in euhedral tourmaline found in the zones and in the pockets. Inspection of Figure 3 allows two areas to be identified, schorl–dravite, related to crystals from *Bz* to *MIz*, and schorl–elbaite for *IIz* and pockets tourmaline. This is in accord with the distribution of unit-cell dimensions (Fig. 2).

Thirty-five samples of tourmaline were chosen as representative of the chemical variation in dykes 1 and 3, and their compositions are presented in Tables 2, 3 and 4. The cation distribution was accomplished according to the general formula [Deer *et al.* (1986), Foit (1989), and references therein; MacDonald *et al.*

TABLE 4. REPRESENTATIVE ELECTRON AND ION MICROPROBE DATA OF ZONED TOURMALINES FROM THE CRUZEIRO PEGMATITE DYKES

Samples	84		93		62			64		
	core	rim	core	rim	core	mantle	rim	core	mantle	rim
SiO_2	35.28	36.36	34.85	36.65	37.40	37.62	38.34	37.80	37.76	38.80
TiO_2	0.04	0.06	0.12	0.05	0.08	0.14	0.09	-	0.22	0.07
B_2O_3	10.35	10.59	10.26	10.64	10.83	10.87	11.04	10.91	10.91	11.14
Al_2O_3	36.37	37.74	34.04	36.73	38.06	39.15	40.10	38.57	38.65	39.65
FeO	8.86	5.56	13.12	6.03	1.45	2.33	1.15	0.97	2.56	0.93
MnO	1.44	1.42	0.80	1.12	3.55	1.83	0.87	3.38	1.35	0.92
MgO	0.40	0.20	-	0.16	-	0.36	0.42	-	0.41	0.16
ZnO	0.33	0.27	0.64	0.25	0.16	-	-	-	-	-
CaO	0.02	0.09	0.05	0.22	0.43	0.17	0.19	0.45	0.28	0.30
Na_2O	2.29	2.57	1.94	2.67	2.37	2.29	2.08	2.33	2.38	2.01
K_2O	0.03	0.02	0.05	0.04	0.04	0.03	0.03	0.04	-	0.03
Li_2O	0.95	1.46	0.52	1.24	1.61	1.64	1.80	1.82	1.84	1.87
F	1.03	1.41	0.76	1.33	1.49	1.26	0.99	1.26	1.11	1.05
H_2O	3.13	3.12	3.00	3.00	3.16	3.22	3.43	3.28	3.33	3.52
Sum	100.53	100.86	100.16	100.12	100.63	100.90	100.53	100.82	100.80	100.45
O=F	-0.43	-0.59	-0.32	-0.56	-0.63	-0.53	-0.42	-0.53	-0.47	-0.44
Total	100.10	100.27	99.84	99.56	100.00	100.37	100.11	100.29	100.33	100.01
Number of ions on the basis of 31 (O,OH,F)										
Si	5.835	5.886	5.905	5.989	5.992	5.971	6.018	6.006	5.987	6.077
Al(*T*)	0.165	0.114	0.095	0.011	0.008	0.029	0.000	0.000	0.013	0.000
B	2.954	2.959	3.000	3.000	2.994	2.978	2.991	2.992	2.985	3.011
Al(*Z*)	6.000	6.000	6.000	6.000	6.000	6.000	6.000	6.000	6.000	6.000
Al(*Y*)	0.927	1.089	0.703	1.063	1.179	1.297	1.421	1.226	1.213	1.322
Fe	1.226	0.752	1.859	0.823	0.194	0.309	0.151	0.129	0.339	0.122
Ti	0.005	0.007	0.015	0.007	0.010	0.017	0.010	0.000	0.026	0.008
Mn	0.202	0.195	0.115	0.155	0.482	0.246	0.115	0.456	0.182	0.122
Mg	0.098	0.049	0.000	0.040	0.000	0.084	0.099	0.000	0.096	0.037
Zn	0.040	0.033	0.081	0.030	0.018	0.000	0.000	0.000	0.000	0.000
Li	0.632	0.951	0.354	0.815	1.039	1.047	1.138	1.164	1.174	1.179
Y tot.	3.130	3.076	3.128	2.932	2.922	3.001	2.935	2.975	3.031	2.790
Ca	0.004	0.015	0.009	0.038	0.074	0.029	0.031	0.077	0.047	0.050
Na	0.735	0.808	0.638	0.847	0.735	0.705	0.633	0.718	0.732	0.610
K	0.006	0.004	0.010	0.007	0.008	0.006	0.006	0.008	0.000	0.006
X tot.	0.746	0.827	0.658	0.892	0.817	0.740	0.670	0.803	0.779	0.666
OH	3.449	3.366	3.390	3.270	3.377	3.410	3.592	3.477	3.522	3.683
F	0.537	0.722	0.407	0.686	0.754	0.632	0.494	0.634	0.555	0.520
OH+F	3.986	4.088	3.797	3.955	4.131	4.042	4.085	4.110	4.077	4.202

B_2O_3, Li_2O and H_2O from ion microprobe. Total iron as FeO. - : Below detection limit. See text for average experimental errors.

(1993)] of the tourmaline group: $XY_3Z_6B_3T_6O_{27}(O,OH)_3(O,OH,F)$, where $X = {}^{[9]}$(Na, K, Ca, □), $Y = {}^{[6]}$(Mg, Fe^{2+}, Mn, Zn, Al + Li, Fe^{3+}, Ti), $Z = {}^{[6]}$(Al, Al + Mg, Fe^{3+}) and $T = {}^{[4]}$(Si, Al).

In Tables 2, 3 and 4, iron content is referred to as FeO_{tot}, because the results obtained show that, for the most part, Fe is in the ferrous state. The few analyses done indicate that Fe_2O_3 varies in schorl from zero (sample 92) to 2.0 wt.% (sample 91), whereas in the Fe-rich elbaite, Fe_2O_3 is undetectable. The shortage of material available for analysis and, above all, the difficulties in preventing oxidation during the long dissolution times required for tourmaline, did not allow FeO to be determined for the whole sample set.

Composition of tourmalines from dykes 1 and 3

The most significant chemical variations of tourmaline from both sides of dyke 1 (Fig. 4) are shown by the *Y*-site cations (Fe, Mg, Al, Li, Zn, Mn) and the anions (OH, F). The same element variations occur for the tourmaline crystals of the western side of dyke 3 (Fig. 5). Inspection of elemental trends of Figures 4 and 5 shows common similarities and differences between dykes 1 and 3. In particular:

(i) the aluminum content is high in schorl composition for dykes 1 and 3, whereas in pockets of dyke 3 it does not reach the values observed in dyke 1;

(ii) the content of iron is particularly high in the inner

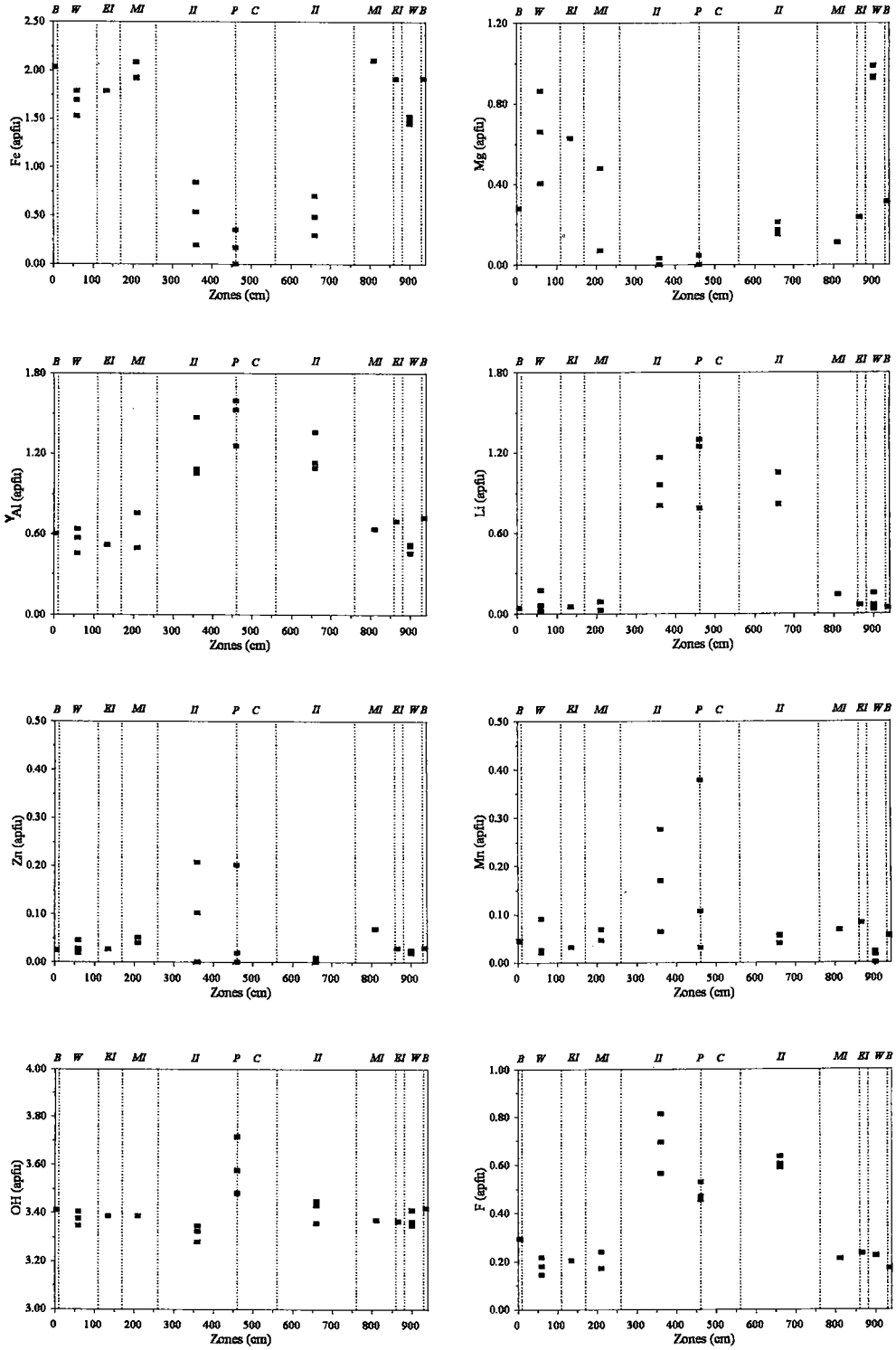

FIG. 4. Compositional variation trends of tourmaline-group minerals at Cruzeiro with respect to their position from western (left) to eastern zones (right) of dyke 1. Data from the representative compositions of Table 2.

zone of dyke 3, where large amounts of huge crystals of schorl are found. In addition, the elbaitic rim of these crystals (as in sample 93) does not show the high Li content and Zn enrichment of the elbaite crystals from dyke 1;

(iii) the levels of magnesium and titanium (Tables 2 and 3) reach their highest values in *Wz* of both dykes;

(iv) the levels of lithium, as of aluminum, do not reach in dyke 3 the values shown in dyke 1;

(v) zinc enrichment is characteristic of the strictly elbaitic composition of the western side of dyke 1;

(vi) manganese enrichment is common to inner zones of both dykes;

(vii) fluorine reaches its highest values in *IIz* of dyke 1 and in the pockets of dyke 3;

(viii) hydroxyl reaches its highest values in pockets of both dykes.

Finally, the Na content of the *X* site does not show a definite trend, its values ranging from 0.54 to 0.87 *apfu* (atoms per formula unit). Since the Ca and K contents are negligible and no other cations are of importance at this site (Lucchesi *et al.*, in prep.), the proportion of vacancies becomes significant in Na-depleted samples.

Figure 4 also allows comparison between tourmaline compositions from western and eastern sides of dyke 1. In particular, in spite of the symmetry shown by most of elements, compositions of western-side tourmaline from the *IIz* have higher Li, Zn, Mn and F than those of the opposite side (Table 2). Zn reaches values up to 2.02 wt.% ZnO (0.25 *apfu*), among the highest values recorded in the literature. Because of their Fe content and lack of Zn, eastern-side elbaite, therefore, shows significant similarities with the pocket elbaite of dyke 3 (Table 3, Fig. 5).

Composition of color-zoned crystals

Euhedral centimetric crystals with marked color-zoning occur in dykes 1 and 3. Sample 84, from *EIz*, and samples 62 and 64, from a pocket, were collected from dyke 1, and sample 93 was collected from the *IIz* of dyke 3. Both samples 93 and 84 (Table 4) show a predominant schorl component in the black core and a significant amount of elbaitic component in the rim. The *Y*-cation trends show a sharp drop in Fe from core to rim, with simultaneous increase in ^{Y}Al (Fig. 6a) and Li. Moreover, in sample 93, Zn decreases sharply from core to rim, whereas Mn increases more subtly (Fig. 6b). No well-defined trends for Zn and Mn are observed in sample 84. Inspection of the data in Table 4 shows that fluorine and hydroxyl behave in an inverse manner: F increases and OH decreases from core to rim.

Core–mantle–rim trends of samples 62 and 64 (Table 4, Fig. 6c) show enrichment in elbaitic component toward the rim, whereas their core and mantle, respectively, are characterized by high Mn and Fe values: up to 3.55 wt.% MnO (0.48 *apfu* Mn) and up to 2.56 wt.% FeO (0.34 *apfu* Fe). Regarding F and OH, the opposite behavior with respect to samples 93 and 84 is observed: F is high in the core, whereas OH is typically enriched in the rim (Table 4).

The composition of zoned crystals of tourmaline shows characteristics that allow comparison between their core–rim trends and the elemental trends along the pegmatite dykes. In particular, core-to-rim trends of schorl samples 84 and 93 (Table 4, Fig. 6a) reflect the elemental variation from the *Bz* to the *IIz* (Figs. 4, 5), whereas those of elbaite samples 62 and 64 (Table 4, Fig. 6c) reflect the chemical evolution from the *IIz* to the pocket in dyke 1 (Fig. 4), especially in terms of F and OH.

Discussion

(OH + F) excess and bond-valence sum calculations

In Tables 2, 3 and 4, the (OH + F) contents in some cases exceed the ideal value of 4.00 *apfu* (Fig. 7). The H_2O excess was already pointed out by Foit & Rosenberg (1977) in a systematic study of tourmaline chemistry based on literature data.

For tourmaline, bond-valence sum (BVS) calculations on anion sites (Donnay & Allmann 1970) yield values close to 2.0 *vu* (valence units) where the sites host oxygen atoms, and values of less than 2.0 *vu* in the presence of other anions such as OH and F.

For the Cruzeiro suite of tourmaline crystals, bond-valence calculations were accomplished using the parameters from Brese & O'Keeffe (1991) and the interatomic distances obtained from 18 structure refinements with *R* values from 1.9 to 3.0% (Lucchesi *et al.*, in prep.). Calculations gave values close to 2.0 *vu* for anion sites from O(4) to O(8), and values lower than 2.0 *vu* not only for O(1) and O(3), as would be expected from the literature, but also for O(2). In the tourmaline structure, the O(3) site hosts only OH (except in buergerite, olenite, and povondraite), and O(1) can host O, OH and F (Grice & Ercit 1993, Grice *et al.* 1993, Gorskaya *et al.* 1982, Barton 1969). The BVS calculations for the Cruzeiro tourmaline crystals of dyke 1 (Fig. 8a) confirm the occupancy of the O(3) site by OH, as the mean value obtained is 1.10 *vu*, and the occupancy of the O(1) site mainly by F and OH, with values ranging from 0.95 to 1.33 *vu* for elbaite and schorl samples, respectively.

The O(2) site should be occupied by an oxygen atom, so its BVS should approach 2.0 *vu*. The calculated BVS values decrease from schorl and Fe-rich elbaite to elbaite, with less than 2.0 *vu* for almost pure elbaite. For tourmaline crystals with (OH + F) higher than 4.00 *apfu*, the values reach a minimum of 1.88 *vu* and are inversely correlated with (OH + F) contents (Fig. 8b). This suggests a partial occupancy of the O(2) site

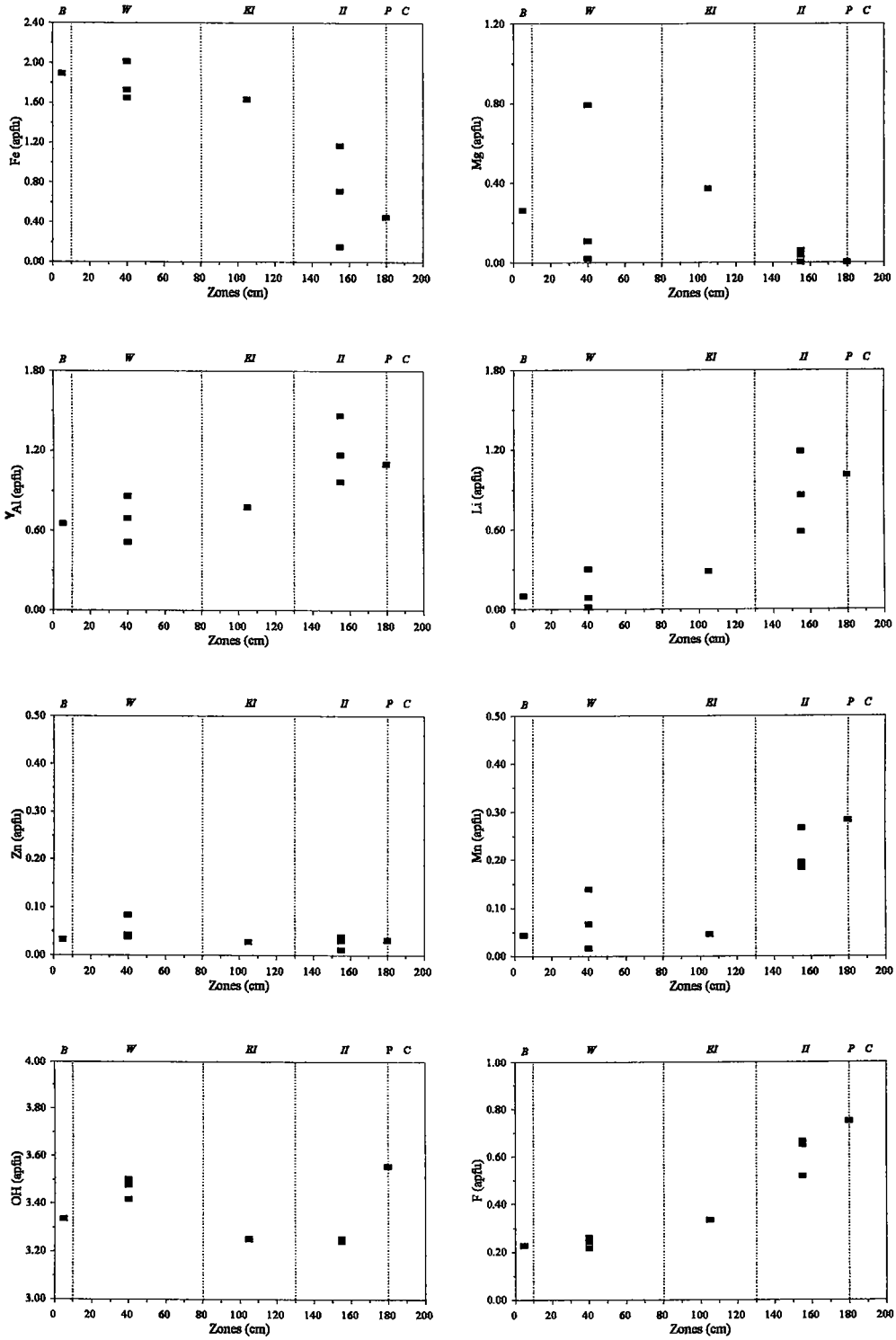

FIG. 5. Compositional variation trends of tourmaline-group minerals at Cruzeiro with respect to their position from western (left) zones to core (right) of dyke 3. Data from the representative compositions of Table 3.

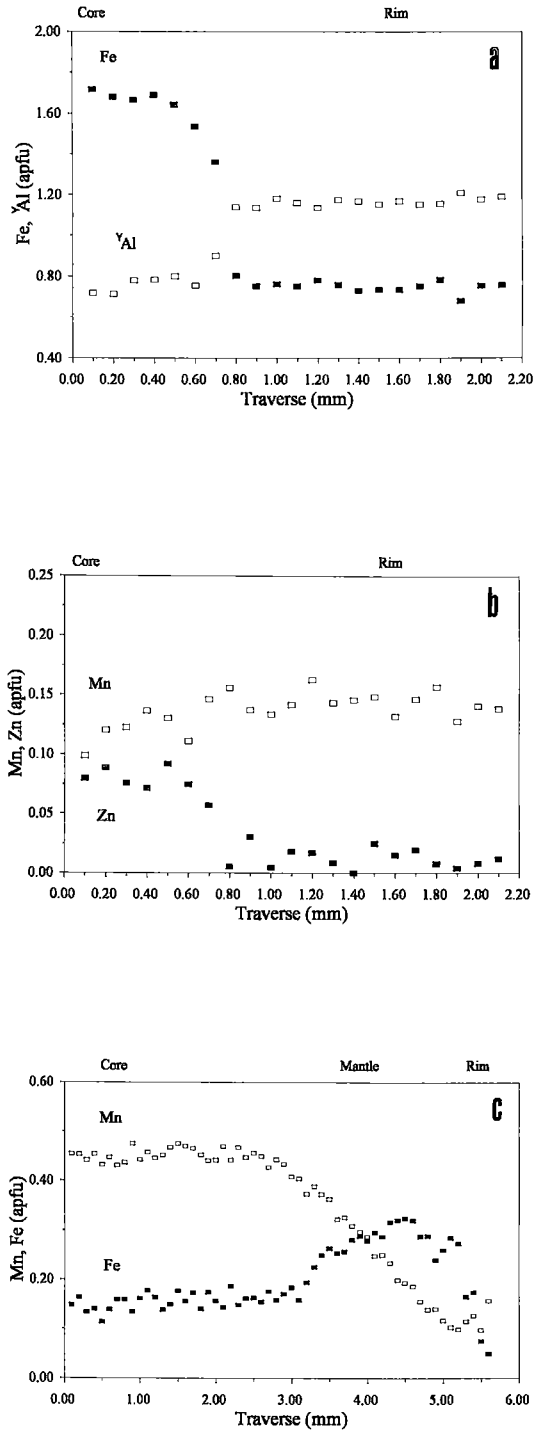

FIG. 6. Electron-microprobe traverses showing trends in the zoned crystals: (a) sample 93, Fe and ^{Y}Al; (b) sample 93, Mn and Zn; (c) sample 64, Mn and Fe.

by OH, a hypothesis already proposed by Hawthorne (1996) on the basis of stereochemical considerations. As OH-rich tourmaline crystals come mainly from pockets formed in the late stages of crystallization, the presence of OH at O(2) could be a response to the growth environment.

Mechanisms of substitution

Compositional variations in tourmaline from the Cruzeiro granitic pegmatites are shown in Figure 3. Coupled substitutions that refer either to the schorl or to the elbaite across the pegmatite dykes, are defined as "general", whereas those that characterize the features of tourmaline from a single pegmatite zone are defined as "specific". They are written as suggested by Henry & Dutrow (1990, Table II) and Burt (1989). The variation of monovalent cations and anions (R^{+} + OH + F) with trivalent cations (R^{3+}) for all samples allows identification of two clusters alongside end-member trends (Fig. 9a).

General substitutions: For schorl compositions (in addition to ^{Y}Mg ↔ ^{Y}Fe), the general substitutions are

$$^{Y}Al^{3+} + O^{2-} \leftrightarrow {}^{Y}Fe^{2+} + OH^{-} \quad AlO(FeOH)_{-1} \quad (1)$$

$$^{X}\square + {}^{Y}Al^{3+} \leftrightarrow {}^{X}Na^{+} + {}^{Y}Fe^{2+} \quad {}^{X}\square Al(NaFe)_{-1} \quad (2).$$

The first substitution produces "proton-deficient schorl", whereas the second substitution produces foitite, $\square[Fe^{2+}_2(Al,Fe^{3+})]Al_6Si_6O_{18}(BO_3)_3(OH)_4$ (MacDonald *et al.* 1993). The following substitution (Foit *et al.* 1989) is also present, although to a lesser extent:

$$^{Y}Al^{3+} + {}^{T}Al^{3+} \leftrightarrow {}^{Y}Fe^{2+} + {}^{T}Si^{4+} \quad Al_2(FeSi)_{-1} \quad (3).$$

Starting from the elbaite end-member, the main general substitution is $2^{Y}R^{2+} \leftrightarrow {}^{Y}Al + {}^{Y}Li$ (with R^{2+} = Fe, Mn, Zn). Another general mechanism to be emphasized is

$$2^{X}\square + {}^{Y}Al^{3+} \leftrightarrow 2^{X}Na^{+} + {}^{Y}Li^{+} \quad {}^{X}\square_2AlNa_{-2}Li_{-1} \quad (4),$$

which implies the presence of the "alkali-free elbaite" component. It accounts for the Al excess with respect to Li at the *Y* site and the lack of Na at the *X* site. As mentioned by Foit & Rosenberg (1977), this substitution is not commonly found in elbaite.

Specific substitutions: In the *Bz*, *Elz*, and *Mlz* the tourmaline substitutions can be fully described with the general mechanisms indicated above for schorl.

In the *Wz*, the dravite substitution reaches its highest extent (Mg up to 0.99 *apfu*), and the presence of Ti (even if in a small quantity) requires the specific mechanism

$$^{Y}Ti^{4+} + 2\,{}^{T}Al^{3+} \leftrightarrow {}^{Y}Fe^{2+} + 2{}^{T}Si^{4+} \quad TiAl_2Fe_{-1}Si_{-2} \quad (5)$$

which could be considered simply a variation of mechanism (3) (Foit *et al.* 1989).

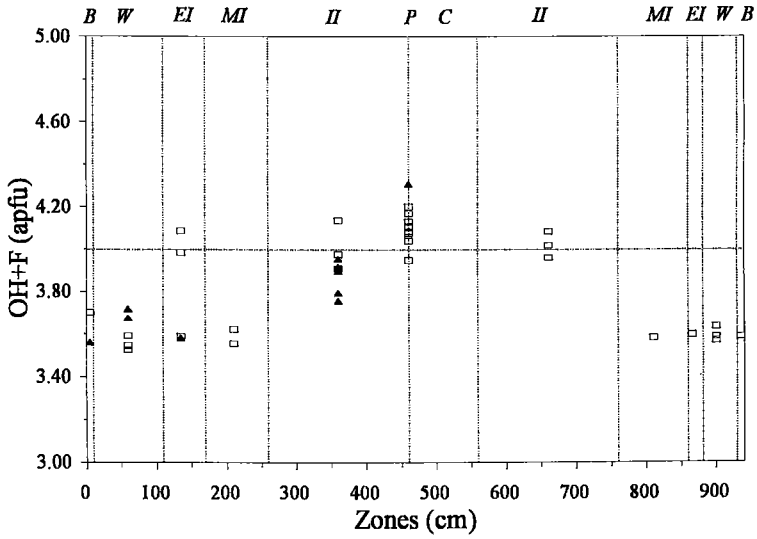

FIG. 7. Variation in (OH + F) in tourmaline crystals from dyke 1 (open squares) and dyke 3 (full triangles) with respect to their position in the pegmatite zones. Tourmaline samples from the *IIz* and pockets show the highest (OH + F) values, locally exceeding the stoichiometric value of 4.00 *apfu*. Owing to differences in relative dimensions between the zones of the two dykes, the position of data from tourmalines of dyke 3 are indicative only.

In the *IIz*, the general substitution $2^{Y}R^{2+} \leftrightarrow {}^{Y}Al + {}^{Y}Li$ reaches its highest extent (Fe + Mg + Mn + Zn = 1.45 *apfu*) and, in addition, the specific mechanism

$$^{Y}Al^{3+} + 2O^{2-} \leftrightarrow Li^{+} + 2OH^{-} \qquad AlO_2Li_{-1}OH_{-2} \quad (6)$$

generates a variable content of the "proton-deficient elbaite" end-member.

In pocket elbaite, several mechanisms are operative:

(i) in crystals 62 and 64:

$$^{Y}\square + OH^{-} \leftrightarrow {}^{Y}Li^{+} + O^{2-} \qquad {}^{Y}\square OH(LiO)_{-1} \quad (7)$$

(ii) in sample 65, the proton-deficient substitution (6) was found, as was the case for elbaite from the *IIz*;

(iii) for samples 60, 61 R, 62 mantle, and 64 mantle, in addition to known end-members, the OH excess could be related to *X*-site vacancy by the following mechanism:

$$^{X}\square + OH^{-} \leftrightarrow {}^{X}Na^{+} + O^{2-} \qquad {}^{X}\square OH(NaO)_{-1} \quad (8)$$

trending toward an "alkali-free proton-rich elbaite" end-member (Fig. 9b);

(iv) sample 95, in particular, exhibits (OH + F) excess (0.31 *apfu*) corresponding to its *Y*- and *X*- site vacancies: therefore, it is reasonable to assume that the octahedral-cation-deficient elbaite (7) and alkali-free proton-rich elbaite (8) end-members act together to produce the OH excess.

Tourmaline composition related to internal evolution of the Cruzeiro dykes

The composition of toumaline in granitic pegmatites is related to melt composition (London 1986) and interactions between pegmatite-forming melt and country rock (Henry & Guidotti 1985, Shearer *et al.* 1986). At Cruzeiro, country-rock interactions can be considered negligible, as the bodies of pegmatite are emplaced in quartzite. The chemical variation of tourmaline is thus due to the internal evolution of the melt–fluid system.

The ubiquitous assemblage of muscovite and tourmaline indicates the peraluminous character of the early pegmatite-forming melt. The high Li content in the elbaite of the *IIz* and pockets, and the presence of abundant spodumene in dyke 1, suggest that the parent melt of dyke 1 was slightly more evolved than that of dyke 3. A disequilibrium fractional-crystallization process through liquidus undercooling (London 1992) is considered responsible for internal zoning of the pegmatite. The compositional variations of tourmaline observed in the Cruzeiro suite from the *Bz* inward reflect the thermal history of the pegmatite system. In particular, the behavior of the *Y*-site cations (including Zn and Mn) shows strong similarities with the ideal covariation of these elements in response to both decreasing temperature and increasing fractionation of the melt (Jolliff *et al.* 1986). The "compositional

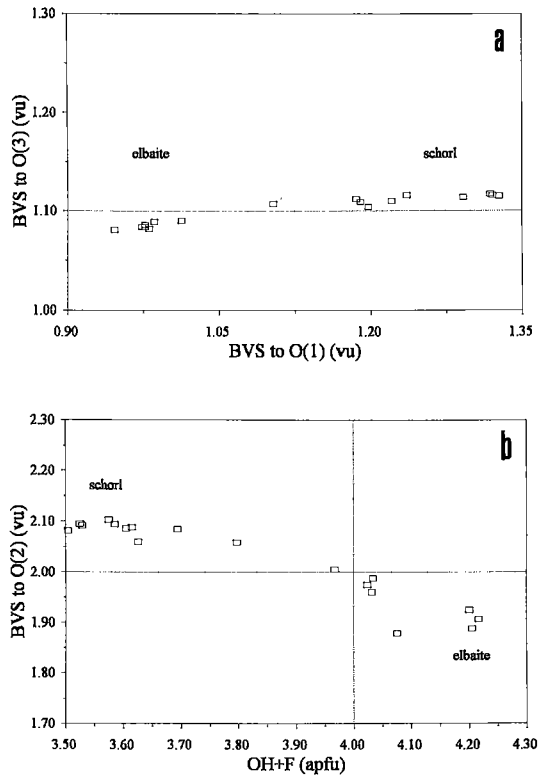

FIG. 8. Bond-valence sums (BVS), expressed as valence units (*vu*), to anion sites of tourmaline in dyke 1. (a) Plot of BVS to O(3) *versus* BVS to O(1). Horizontal line outlines the mean value (1.10 *vu*) of BVS to O(3). (b) Plot of BVS to O(2) *versus* (OH + F) contents. BVS values higher than 2.0 *vu* are from schorl, those values on or around 2.0 *vu* are from Fe-rich elbaite, and values lower than 2.0 are from pure elbaite.

asymmetry" in tourmaline from the western and eastern sides of dyke 1 can be explained by upward movement of an evolved melt rich in H_2O, Li, B, F, Mn and Zn during the late stages of the solidification process. This is in accord with the enrichment of Li-, F- and OH-minerals in the upper part of the pegmatite dyke (César-Mendes *et al.* 1993a), and could have produced the concentration of incompatible elements toward the western side of the solidifying dyke because of its southwesterly dip.

The relation between the stability of Li-minerals and F activity implies the crystallization of spodumene in F-poor environments (Černý & Burt 1984) and the deposition of lepidolite in the case of high activity of F (Heinrich 1967). In dyke 1 at Cruzeiro, the high Li and low F contents in the melt are recorded by ubiquitous F-poor tourmaline and large amounts of spodumene near the core.

CONCLUDING REMARKS

With continuous crystallization of pegmatite, *general substitutions* produce proton-deficient schorl (eq. 1) and alkali-free schorl (eq. 2) in the outer zones, and alkali-free elbaite (eq. 4) in the inner zones.

Specific substitutions characterize the *Wz* schorl, in which ^{T}Al balances ^{Y}Ti (eq. 5), and the *IIz* and pocket elbaite, in which compositions trend toward proton-deficient elbaite (eq. 6). Moreover, in pocket elbaite, distinct crystals exhibit particular substitutions such as the octahedral-defect type (eq. 7), which explains OH excess and vacancies at the *Y*-site, and the proposed alkali-free proton-rich type (eq. 8), which explains OH excess and vacancy at the *X*-site. These latter mechanisms characterize tourmaline from particular environments, in which a supercritical aqueous fluid was plentiful (*e.g.*, pegmatite pockets). This OH excess in tourmaline structure occurs at the O(2) site. It should also be noted that, *via* the proposed mechanism (8), the deficit of Na at the *X* site seems to be related to the partial occupancy of O(2) by excess OH. Finally, the compositional trends of zoned crystals from both intermediate zones and pockets record the chemical variations in tourmaline across the whole pegmatite.

Assuming the "disequilibrium fractional-crystallization model" (London 1992) to account for the internal zoning, the evolutionary features shown by the composition of tourmaline from the *Bz* to pockets suggest the following features of melt evolution:

(1) Tourmaline crystals display Al enrichment, reflecting the abundance of this element in the melt.

(2) Systematic changes in *Y*-site cations from the *Bz* to the pockets indicate that Mg, Fe, Zn, Mn and Li reached their maximum in activity at different stages of pegmatite evolution.

(3) Crystallization of large quantities of tourmaline in the *IIz* removed large amounts of boron from the melt and lowered the solubility of H_2O. This accounts for the exsolution of an H_2O-rich fluid, responsible for pocket formation and late crystallization of OH-rich tourmaline.

(4) The "compositional asymmetry" displayed by the tourmaline crystals from the western and the eastern sides of dyke 1 enabled the late stages of melt consolidation of the pegmatite to be reconstructed.

(5) The low F content of tourmaline in this suite reflects limited F activity in the volatile phase and in the melt, further confirmed by the stability of spodumene both in the *IIz* and in the pockets.

ACKNOWLEDGEMENTS

The manuscript benefitted from a review by P. Černý, to whom the authors are indebted. J. MacManus revised the English text. M. Serracino is thanked for

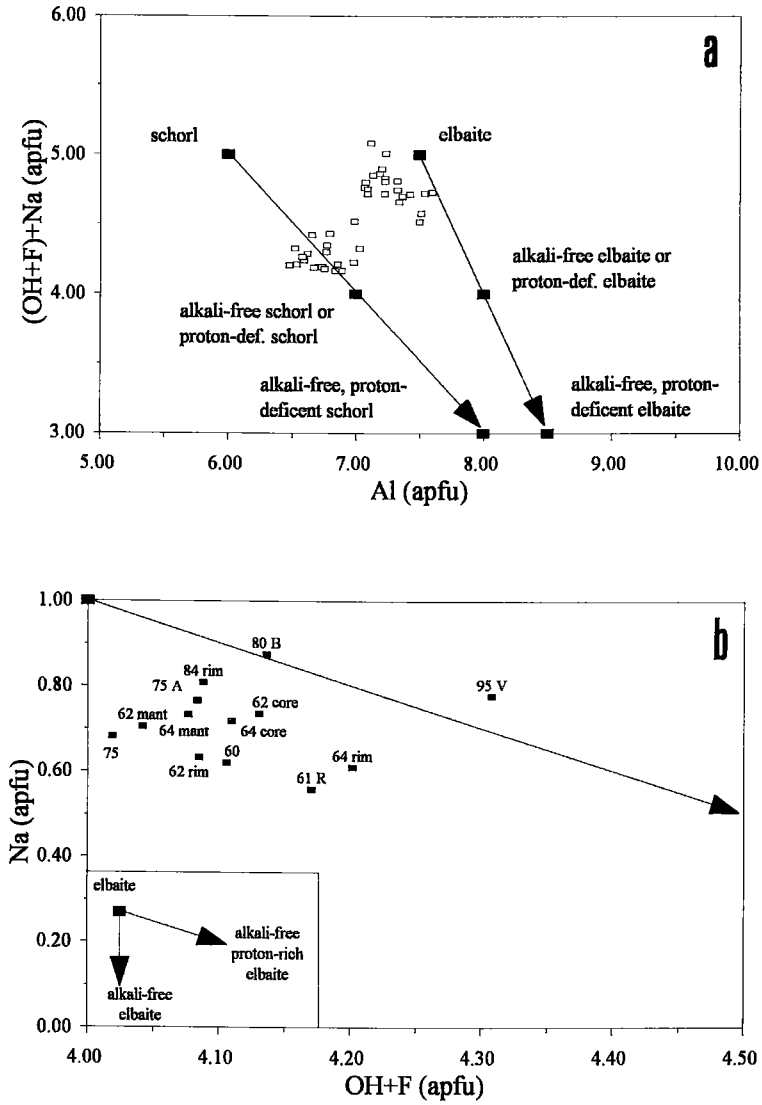

FIG. 9. Schemes of coupled substitution in tourmaline crystals at Cruzeiro. (a) Plot of (OH + F) + Na *versus* Al. The diagram shows how the Cruzeiro samples compare to ideal trends for schorl and elbaite. (b) Plot of Na *versus* (OH + F). The diagram shows that in OH-rich elbaite, the Na deficiency is balanced by OH excess.

his assistance during the collection of the electron-microprobe data. This work was supported by a MURST grant. Final reviews by F.C. Hawthorne and F.F. Foit Jr. are gratefully acknowledged.

References

BARTON, R., JR. (1969): Refinement of the crystal structure of buergerite and the absolute orientation of tourmalines. *Acta Crystallogr.* **B25**, 1524-1533.

BRESE, N.E. & O'KEEFFE, M. (1991): Bond-valence parameters for solids. *Acta Crystallogr.* **B47**, 192-197.

BURT, D.M. (1989): Vector representation of tourmaline compositions. *Am. Mineral.* **74**, 826-839.

CASSEDANNE, J.P., CASSEDANNE, J.O. & SAUER, D.A. (1980): Famous mineral localities: the Cruzeiro mine past and present. *Mineral. Rec.* **11**, 363-370.

ČERNÝ, P. & BURT, D.M. (1984): Paragenesis, crystallochemical characteristics, and geochemical evolution of micas in granite pegmatites. *In* Micas (S.W. Bailey, ed.). *Rev. Mineral.* **13**, 257-297.

CÉSAR-MENDES, J. (1995): *Mineralogia e gênese dos pegmatitos turmaliníferos da Mina do Cruzeiro, São José da Safira, Minas Gerais*. Tese de Doutoramento, Univ. São Paulo, São Paulo, Brazil.

_____, BOTELHO, N.F. & SVISERO, D.P. (1993a): Polilithionita: uma mica rara no pegmatito do Cruzeiro, São José da Safira, Minas Gerais. *In* Cong. Bras. Geoq. 4 (Brasilia). *Bol. Res. Expand A.B.N.T., Brasilia*, SBG **1**, 164-166 (abstr.).

_____, CORREIA-NEVES, J.M. & SVISERO, D.P. (1993b): Aspectos mineralógicos e geoquímicos dos niobio-tantalatos do Pegmatito do Cruzeiro, São José da Safira, Estado de Minas Gerais, Brasil. *In* Cong. Geoq. Paises de Lingua Portuguesa II (Porto, Portugal). *Memorias do Museu do Laboratório Mineralógico e Geológico da Universidade do Porto* **1**, 209-213.

_____ & JORDT-EVANGELISTA, H. (1994): Pegmatitos da região de São José da Safira, MG: origem anatéctica ou granitica? *In* Cong. Bras. Geol. 38 (Balneário Camboriú). *Bol. Res. Expand A.B.N.T., Balneário Camboriú*, SBG. **3**, 95-96 (abstr.).

_____ & SVISERO, D.P. (1992): Aspectos geoquímicos das granadas da Jazida de turmalina do Cruzeiro, Municipio de São José da Safira, Estado de Minas Gerais. *In* Cong. Bras. Geol. 37 (São Paulo). *Bol. Res. Expand A.B.N.T., São Paulo*, SBG. **2**, 2-3 (abstr.).

_____ & _____ (1994): Evolução geoquímica das micas do Pegmatito do Cruzeiro, São José da Safira, Estado de Minas Gerais. *In* Cong. Bras. Geol. 38 (Balneário Camboriú). *Bol. Res. Expand A.B.N.T., Balneário Camboriú*, SBG **3**, 143-144 (abstr.).

DEER, W.A., HOWIE, R.A. & ZUSSMAN, J. (1986): *Disilicates and Ring Silicates*. **1B** (2nd ed.). Longman, Harlow, U.K.

DELOULE, E., CHAUSSIDON, M. & ALLÉ, P. (1992): Instrumental limitations for isotope ratios measurements with a Cameca IMS-3f ion microprobe: example of H, B, S and Sr. *Chem. Geol.* **101**, 187-192.

DONNAY, G. & ALLMANN, R. (1970): How to recognize O^{2-}, OH^- and H_2O in crystal structures determined by X-rays. *Am. Mineral.* **55**, 1003-1015.

FOIT, F.F., JR. (1989): Crystal chemistry of alkali-deficient schorl and tourmaline structural relationships. *Am. Mineral.* **74**, 422-431.

_____, FUCHS, Y. & MYERS, P.E. (1989): Chemistry of alkali-deficient schorls from two tourmaline – dumortierite deposits. *Am. Mineral.* **74**, 1317-1324.

_____ & ROSENBERG, P.E. (1977): Coupled substitutions in the tourmaline group. *Contrib. Mineral. Petrol.* **62**, 109-127.

FOORD, E.E. (1977): Famous mineral localities: the Himalaya dyke system, Mesa Grande District, San Diego, California. *Mineral. Rec.* **8**, 461-474.

_____, SPAULDING, L.B., JR., MASON, R.A. & MARTIN, R.F. (1989): Mineralogy and paragenesis of the Little Three mine pegmatites, Ramona district, San Diego County, California. *Mineral. Rec.* **20**, 101-127.

GORSKAYA, M.G., FRANK-KAMENETSKAYA, O.V., ROZHDESTVENSKAYA, I.V. & FRANK-KAMENETSKII, V.A. (1982): Refinement of the crystal structure of Al-rich elbaite, and some aspects of the crystal chemistry of tourmalines. *Sov. Phys. Crystallogr.* **27**, 63-66.

GRICE, J.D. & ERCIT, T.S. (1993): Ordering of Fe and Mg in the tourmaline crystal structure: the correct formula. *Neues Jahrb. Mineral. Abh.* **165**, 245-266.

_____, _____ & HAWTHORNE, F.C. (1993): Povondraite, a redefinition of the tourmaline ferridravite. *Am. Mineral.* **78**, 433-436.

HAWTHORNE, F.C. (1996): Structural mechanisms for light-element variations in tourmaline. *Can. Mineral.* **34**, 123-132.

HEINRICH, E.W. (1967): Micas of the Brown Derby pegmatites, Gunnisan County, Colorado. *Am. Mineral.* **52**, 1110-1121.

HENRY, D.J. & DUTROW, B.L. (1990): Ca substitution in Li-poor aluminous tourmaline. *Can. Mineral.* **28**, 111-124.

_____ & GUIDOTTI, C.V. (1985): Tourmaline as a petrogenetic indicator mineral: an example from the staurolite-grade metapelites of NW Maine. *Am. Mineral.* **70**, 1-15.

JOLLIFF, B.L., PAPIKE, J.J. & SHEARER, C.K. (1986): Tourmaline as a recorder of pegmatite evolution: Bob Ingersoll pegmatite, Black Hills, South Dakota. *Am. Mineral.* **71**, 472-500.

LONDON, D. (1986): Formation of tourmaline-rich gem pockets in miarolitic pegmatites. *Am. Mineral.* **71**, 396-405.

_____ (1992): The application of experimental petrology to the genesis and crystallization of granitic pegmatites. *Can. Mineral.* **30**, 499-540.

MACDONALD, D.J., HAWTHORNE, F.C. & GRICE, J.D. (1993): Foitite, $\square[Fe^{2+}_2(Al,Fe^{3+})]Al_6Si_6O_{18}(BO_3)_3(OH)_4$, a new alkali-deficient tourmaline: description and crystal structure. *Am. Mineral.* **78**, 1299-1303.

SHEARER, C.K., PAPIKE, J.J., SIMON, S.B. & LAUL, J.C. (1986): Pegmatite – wallrock interactions, Black Hills, South Dakota: interaction between pegmatite-derived fluids and quartz–mica schist wallrock. *Am. Mineral.* **71**, 518-539.

SILVA, J.M.R., LIMA, M.I.C., VERONESE, V.F., RIBEIRO JUNIOR, R.N., ROCHA, R.M. & SIGA JUNIOR, O. (1987): *In* Projeto Radambrasil, Folha SE-24: Rio Doce. *IBGE, Rio de Janeiro* **34**, 23-174.

STAATZ, M.H., MURATA, K.J. & GLASS, J.J. (1955): Variation of composition and physical properties of tourmaline with its position in the pegmatite. *Am. Mineral.* **40**, 789-804.

WALKER, R.J., HANSON, G.N., PAPIKE, J.J., O'NEIL, J.R. & LAUL J.C. (1986): Internal evolution of the Tin Mountain pegmatite, Black Hills, South Dakota. *Am. Mineral.* **71**, 440-459.

WILSON, G.C. & LONG, J.V.P. (1983): The distribution of lithium in some Cornish minerals: ion microprobe measurements. *Mineral. Mag.* **47**, 191-199.

Received July 31, 1997, revised manuscript accepted April 7, 1998.